Atmos. Chem. Phys., 7, 5971–5987, 2007
www.atmos-chem-phys.net/7/5971/2007/

Atmospheric Chemistry and Physics

SCIAMACHY tropospheric NO_2 over Switzerland: estimates of NO_X lifetimes and impact of the complex Alpine topography on the retrieval

D. Schaub[1], D. Brunner[1], K. F. Boersma[2], J. Keller[3], D. Folini[1], B. Buchmann[1], H. Berresheim[4,*], and J. Staehelin[5]

[1]Empa, Swiss Federal Laboratories for Materials Testing and Research, Ueberlandstrasse 129, 8600 Duebendorf, Switzerland
[2]School of Engineering and Applied Sciences, Harvard University, Cambridge, Massachusetts, USA
[3]Paul Scherrer Institute (PSI), 5232 Villigen PSI, Switzerland
[4]German National Meteorological Service, DWD/MOHp, 82383 Hohenpeissenberg, Germany
[5]Swiss Federal Institute of Technology (ETH), Universitätstrasse 16, 8092 Zurich, Switzerland
[*]now at: National University of Ireland Galway, Department of Physics, University Road, Galway, Ireland

Received: 23 November 2006 – Published in Atmos. Chem. Phys. Discuss.: 12 January 2007
Revised: 9 November 2007 – Accepted: 21 November 2007 – Published: 7 December 2007

Abstract. This study evaluates NO_2 vertical tropospheric column densities (VTCs) retrieved from measurements of the Scanning Imaging Absorption Spectrometer for Atmospheric Chartography (SCIAMACHY) above Switzerland and the Alpine region. The close correlation between pixel averaged NO_x emission rates from a spatially and temporally highly resolved inventory and the NO_2 VTCs under anticyclonic meteorological conditions demonstrates the general ability of SCIAMACHY to detect sources of NO_x pollution in Switzerland. This correlation is further used to infer seasonal mean NO_x lifetimes carefully taking into account the influence of the strong diurnal cycle in NO_x emissions on these estimates. Lifetimes are estimated to 3.6 ($\pm$0.8) hours in summer and 13.1 ($\pm$3.8) hours in winter, the winter value being somewhat lower than previous estimates. A comparison between the 2003-2005 mean NO_2 VTC distribution over Switzerland and the corresponding 1996–2003 mean from the Global Ozone Monitoring Experiment (GOME) illustrates the much better capability of SCIAMACHY to resolve regional scale pollution features. However, the comparison of seasonal averages over the Swiss Plateau with GOME and ground based in situ observations indicates that SCIAMACHY exhibits a too weak seasonal cycle with comparatively high values in summer and low values in winter. A problem likely contributing to the reduced values in winter (not reported in earlier literature) is the use of inaccurate satellite pixel surface pressures derived from a coarse resolution global model in the retrieval. The marked topography in the Alpine region can lead to deviations of several hundred meters between the model assumed and the real pixel-averaged surface height. A sensitivity study based on selected clear sky SCIAMACHY NO_2 VTCs over the Swiss Plateau and two fixed a priori NO_2 profile shapes indicates that inaccurate pixel surface pressures affect retrieved NO_2 columns over complex terrain by up to 40%. For retrievals in the UV-visible spectral range with a decreasing sensitivity towards the earth's surface, this effect is of major importance when the NO_2 resides close to the ground, a situation most frequently observed during winter.

Correspondence to: D. Brunner
(dominik.brunner@empa.ch)

1 Introduction

Nitrogen dioxide is an important air pollutant. It can affect human health and plays a major role in the production of tropospheric ozone (Seinfeld and Pandis, 1998; Finlayson-Pitts and Pitts, 2000). The bulk of NO_x (NO_x=NO+NO_2) is emitted by the high-temperature combustion of fossil fuel in the highly industrialised continental regions in the northern mid-latitudes. Important natural sources are biomass burning and the microbial production in soils of the non-polar continental surface. At higher altitudes in the troposphere NO_x is directly injected into the troposphere by lightning and aircraft emissions (IPCC, 2001). NO_x is primarily emitted as NO which oxidises to NO_2 within a few minutes. The NO_2 concentration is affected by the partitioning of NO_x into NO and NO_2 which depends on the abundance of ozone and reactive organic compounds as well as on solar light intensity and temperature, and which therefore changes with altitude and with time of day in the troposphere. NO_x is removed from the troposphere mainly by conversion to nitric acid (HNO_3). During daytime, HNO_3 is formed through the

Published by Copernicus Publications on behalf of the European Geosciences Union.

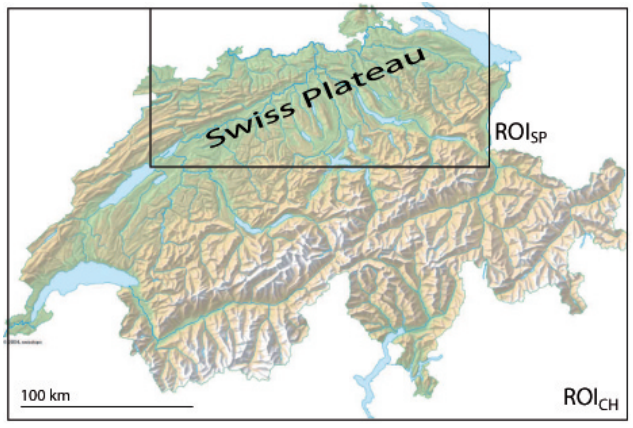

Fig. 1. Regions of interest used in this study covering the whole Switzerland (6° E–10.5° E, 45.75° N–47.75° N, ROI_{CH}) and the polluted Swiss Plateau (7° E–9.5° E, 47° N–47.75° N, ROI_{SP}). (Topographic map of Switzerland: © 2005 swisstopo).

reaction of NO_2 with the OH radical. At night, a two step reaction mechanism forms nitrogen pentoxide (N_2O_5) which further reacts on surfaces and aerosol to HNO_3 (Dentener and Crutzen, 1993). HNO_3 is finally removed by dry and wet deposition (Kramm et al., 1995). Typical lifetimes of NO_x are of the order of 4 to 20 h depending on season (Seinfeld and Pandis, 1998). This is supported by results presented in this study inferred from the combination of SCIAMACHY NO_2 VTCs with a high-quality NO_x emission inventory. The reverse approach, that is the computation of NO_x emissions from satellite column observations based on a priori knowledge of NO_x lifetimes or NO_2 column to NO_x emission ratios taken from a model, has recently become an important tool in top-down emission estimation for regions where sources are not well known (e.g. Martin et al., 2003).

Although the NO_x concentration in Switzerland decreased during the last 15 years the Swiss NO_2 annual ambient air quality standard of 30 μgm^{-3} (≈16 ppb) is still exceeded in polluted areas (FOEN, 2005) and there has been a stagnation or even a slight increase in NO_2 in recent years (Hueglin et al., 2006). Monitoring of nitrogen oxides therefore plays an important role for the assessment of reduction measures. Complementary to ground-based monitoring networks which provide detailed information of local near-surface air pollution, space-borne instruments such as the Global Ozone Monitoring Experiment (GOME) (Burrows et al., 1999) and the Scanning Imaging Absorption Spectrometer for Atmospheric Chartography (SCIAMACHY) (Bovensmann et al., 1999) provide area-wide data of NO_2 vertical tropospheric column densities (VTCs) with global coverage within a few days. The gradually improving resolution of space-borne UV/VIS instruments (GOME pixel size: 320×40 km^2, SCIAMACHY: 60×30 km^2, occasionally 30×30 km^2, Ozone Monitoring Instrument (OMI): up to 13×24 km^2 at nadir) increasingly allows to detect NO_2 pollution features on a regional scale. However, these space-borne data and their complex retrieval are still recent and evolving techniques and validation is therefore needed. Schaub et al. (2006) summarised different validation campaigns of GOME and SCIAMACHY NO_2 data and carried out a detailed comparison of GOME NO_2 VTCs retrieved by KNMI (Royal Dutch Meteorological Institute) and BIRA/IASB (Belgian Institute for Space Aeronomy) with NO_2 profiles derived from ground-based in situ measurements at different altitudes in the Alpine region.

In this paper we evaluate SCIAMACHY NO_2 VTCs over Switzerland and the Alpine region with regard to their use for air quality monitoring and modelling on a regional scale and over a complex topography. The observations are compared to a high quality NO_x emission inventory in order to test the ability of SCIAMACHY to detect the distribution of NO_x pollution sources on the scale of a small country. This comparison is further used to infer seasonal mean NO_x lifetimes carefully taking into account the influence of the strong diurnal cycle in NO_x emissions on these estimates.

The significantly enhanced potential of SCIAMACHY as compared to the Global Ozone Monitoring Instrument GOME regarding the resolution of regional scale NO_x pollution features is demonstrated by a comparison of multi-annual mean distributions of the two instruments over Switzerland. In addition, mean seasonal cycles representative for the Swiss Plateau are calculated for both instruments and compared to each other as well as to NO_2 columns deduced from ground-based in situ measurements carried out at different altitudes. From this comparison evidence is found that SCIAMACHY underestimates the amplitude of the seasonal cycle over the Swiss Plateau.

In the last part of this study the potential effects of the complex topography over the Alpine region on the retrieval are investigated. Based on a sensitivity analysis applied to selected SCIAMACHY pixels it is demonstrated that the use of a coarse resolution topography in the retrieval can indeed lead to significant systematic errors in NO_2 VTCs over the Swiss Plateau. The results are relevant for any region of the globe with a marked orography and highlight the need for a more accurate representation of this parameter in future satellite retrievals.

2 Data

2.1 KNMI/BIRA GOME and SCIAMACHY tropospheric NO_2 observations

Nadir measurements from GOME on board ESA's ERS-2 satellite and from SCIAMACHY on board ESA's Envisat satellite are used in the present study. Depending on whether the focus is the whole domain of Switzerland or only the densely populated Swiss Plateau, our analyses will be

restricted to pixels with centre coordinates within the region of interest ROI_{CH} or ROI_{SP}, respectively (Fig. 1).

The GOME and SCIAMACHY observations are obtained at approximately 10:30 and 10:00 local time and individual pixels cover an area of $320\times40\,km^2$ and $60\times30\,km^2$, respectively. The GOME and SCIAMACHY measurement principles are described in Burrows et al. (1999) and Bovensmann et al. (1999), respectively. The NO_2 VTCs studied in this work are the product of a collaboration between KNMI and BIRA/IASB. Both GOME and SCIAMACHY NO_2 data are publicly available on a day-by-day basis via ESA's TEMIS project (Tropospheric Emission Monitoring Internet Service,www.temis.nl).

The first retrieval step is based on the Differential Optical Absorption Spectroscopy (DOAS) technique (Platt, 1994; Vandaele et al., 2005): a polynomial and a modelled spectrum are fitted to the logarithm of the ratio of earthshine radiance to solar irradiance in the spectral window from 426.3–451.3 nm. The modelled spectrum accounts for spectral absorption features of NO_2, O_3, O_2-O_2, H_2O, and the filling-in of Fraunhofer lines by Raman scattering ("Ring effect"). Scattering by clouds, aerosols, air molecules and the surface is described by a low-order polynomial. This first retrieval step results in the slant column density (SCD) of NO_2, which can be interpreted as the column integral of absorbing NO_2 molecules along the effective photon path from the sun through the atmosphere to the spectrometer.

The second retrieval step separates the stratospheric contribution from the total SCD (Boersma et al., 2004). For KNMI retrievals this is achieved with a data-assimilation approach using the TM4 global chemistry transport model (CTM) (Dentener et al., 2003). The tropospheric SCD (SCD_{trop}) results from the subtraction of the stratospheric estimate from the total SCD.

In the third retrieval step, the SCD_{trop} is converted into a VTC by applying the tropospheric air mass factor (AMF_{trop}). Following Palmer et al. (2001) and Boersma et al. (2004), the retrieved SCIAMACHY NO_2 VTC (X_{SCIA}) is calculated as

$$X_{SCIA}=\frac{N_{trop}}{M_{trop}(\boldsymbol{x}_a,\boldsymbol{b})}=\frac{N_{trop}\cdot\sum_l x_{a,l}}{\sum_l m_l(\boldsymbol{b})\cdot x_{a,l}} \quad (1)$$

where N_{trop} denotes the tropospheric slant column density, M_{trop} the tropospheric air mass factor, $x_{a,l}$ the layer specific subcolumns from the a priori profile x_a, and m_l the altitude-dependent scattering weights. These weights are calculated with the Doubling Adding KNMI (DAK) radiative transfer model (Stammes, 2001) and best estimates for forward model parameters b, describing surface albedo, cloud parameters (fraction, height) and pixel surface pressure. The a priori NO_2 profiles for every location and all times are obtained from the TM4 CTM. Cloud fraction and height are taken from the Fast Retrieval Scheme for Clouds from the Oxygen A band (FRESCO) algorithm (Koelemeijer et al., 2001). Since the TM4 model is driven by meteorological data of the European Centre for Medium-Range Weather Forecasts (ECMWF) the surface pressures in TM4 are taken from the ECMWF model on the $2^\circ\times3^\circ$ resolution of the TM4 model. The surface pressure for an individual satellite pixel is linearly interpolated to the pixel location (hereafter ECMWF/TM4 surface pressure).

The different error sources in tropospheric NO_2 retrievals have been discussed extensively in Boersma et al. (2004) for GOME and error propagation studies have shown that SCIAMACHY errors are similar (Boersma et al., 2007). Based on this work, errors for both GOME and SCIAMACHY NO_2 VTCs are estimated on a pixel-to-pixel basis and additionally provided in the TEMIS data sets. However, these studies have not included the effect of errors in surface pressure. The present work will show that, over a complex topography, an inadequate treatment of this parameter may lead to significant errors which tend to be larger for an instrument with a higher spatial resolution such as SCIAMACHY as compared to GOME.

2.2 Swiss NO_x emissions

Swiss NO_x emissions amount to 33.2 kt N/y with traffic, industry, agriculture/forestry and residential activities contributing 58%, 24%, 12% and 6%, respectively, for the year 2000 (FOEN, 2005). The present study employs an hourly resolved NO_x emission inventory for Switzerland available on a $3\times3\,km^2$ grid. It combines the following basic data sets:

- Road traffic emissions of NO_x for the reference year 2000 with a spatial resolution of 250 m prepared by the consulting company INFRAS, Switzerland. The data set includes an average diurnal variation. Long-term trends of annual totals recently published in Keller and Zbinden (2004) were used to interpolate the emissions between 2000 and 2005.

- NO_x emissions from residential activities, heating, industry, off-road traffic and agriculture/forestry for the reference year 2000 with a spatial resolution of 200 m and accounting for seasonal variations prepared by the company Meteotest, Switzerland. Data sets for other years of interest were calculated on the basis of trends provided by the Swiss Federal Office for the Environment (FOEN, 1995).

Additional information on the emission inventory is summarised in Keller et al. (2005). Total emission inventories are usually based on a large number of input variables. Each of these parameters – and, thus, also the resulting total emission inventory – are affected by uncertainties. Their assessment is a challenging task which needs further assumptions (e.g. Kühlwein and Friedrich, 2000). For the $3\times3\,km^2$ Swiss NO_x emission inventory an accuracy of ±15–20% is estimated in FOEN (1995). Kühlwein (2004) further pointed out increasing errors in emission inventories for increasing spatial resolutions. Thus, due to integration of the $3\times3\,km^2$

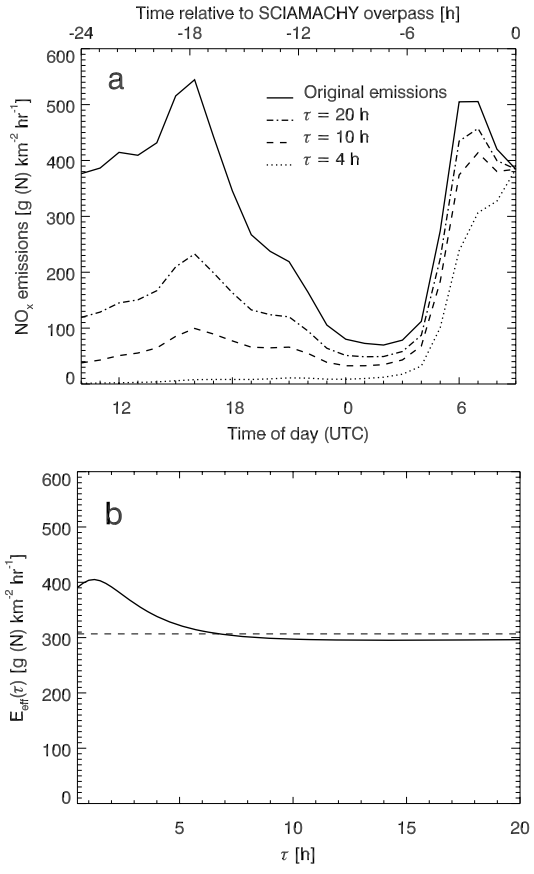

Fig. 2. Diurnal cycle of NO_x emissions (in g (N) km^{-2} h^{-1}) over Switzerland. The solid line is the hourly emission flux from the Swiss emission inventory (in winter) averaged over the domain of Switzerland. The three other lines illustrate the effect of the exponential decay of NO_x for three selected lifetimes τ. This decay leads to a reduced contribution of the emissions released at a given time of the day to the NO_x column M measured at the SCIAMACHY overpass time, see Eq. (5) **(a)**. Effective NO_x emission rate E_{eff} as a function of lifetime τ. The dashed line is the daily mean emission rate (average of solid line if panel a) **(b)**.

resolved emission data over the SCIAMACHY pixel size of $60\times30\,km^2$ in the present work, the above given error of 20% is considered as a reasonable upper limit, which will be assumed in this study.

3 Methods

3.1 Comparison of NO_2 VTCs with a high resolution emission inventory for the estimation of mean NO_x lifetimes

In Sects. 4.1.1 and 4.1.2 NO_2 VTCs will be compared to the Swiss NO_x emission inventory for SCIAMACHY pixels located entirely within the Swiss boundaries. A representative emission rate is computed for each NO_2 VTC by averaging the gridded inventory data over the area of the pixel. The comparison is restricted to clear sky pixels (cloud fraction $<$ 0.1) and anticyclonic conditions. Meteorological conditions are deduced from the Alpine Weather Statistics described in MeteoSwiss (1985). The Alpine Weather Statistics distinguishes between advective and convective classes based on pressure gradients in surface charts. Anticyclonic conditions are a subset of the convective class and are characterized by fair weather and low surface level winds of typically less than 15 km/h. Significant long-range advection of air pollutants is unlikely to occur under these conditions, at least in the boundary layer. Therefore, a close association between the emission distribution and the NO_2 column field is expected.

The NO_x emissions released at the location of the column are considered as the main flux of NO_x into the column which, in an equilibrium state, is balanced by the chemical and physical (i.e. deposition) losses in the column. Neglecting transport and assuming first order losses only and steady state, we can write

$$\frac{dM}{dt} = E - k \cdot M = 0, \tag{2}$$

with M the amount of NO_x in the column (in g (N) km^{-2}), E the NO_x emission flux (in g (N) km^{-2} h^{-1}), and k the first order loss rate. Reforming yields

$$M = \frac{1}{k} \cdot E = \tau \cdot E, \tag{3}$$

with τ the lifetime of NO_x in the column. The lifetime can thus be obtained as the slope in a correlation plot of M versus E. In order to account for inaccuracies in both the observed columns and the emission rates, the slopes are calculated using weighted orthogonal regression (York, 1966). NO_x columns M are computed from the product of SCIAMACHY tropospheric NO_2 VTC and simulated NO_x/NO_2 ratios, both contributing to the error in M. The SCIAMACHY NO_2 VTC 1σ error estimates are taken from the TEMIS data file where error estimates are provided for each individual pixel (Boersma et al., 2004). Errors introduced by the uncertainty in NO_x/NO_2 column ratios are described later. For the NO_x emission fluxes averaged over the individual SCIAMACHY pixels an error of 20% is assumed (Sect. 2.2).

The basic assumption of steady state has also been made in earlier studies by Leue et al. (2001), Beirle et al. (2003) and Kunhikrishnan et al. (2004). It disregards the horizontal NO_x transport into and out of the column. This transport, however, can lead to a smearing because the net effect of transport will be negative for regions with large sources and positive for the surrounding areas. The smearing effect is also depending on the prevailing meteorology (e.g. wind speed and direction) and the chemical lifetime. For mapping isoprene emissions from space-borne data, Palmer et al. (2003) determined typical smearing length scales. For NO_x lifetimes in the order of hours to one day, this length scale is $\sim$100 km (Martin et al., 2003). While neglecting the effect of transport is well justified for the large size of GOME pixels as

in the study of Martin et al. (2003), this might be problematic for SCIAMACHY data with a much smaller pixel size of $60\times30\,km^2$. However, as described above, our analysis is restricted to clear sky pixels and anticyclonic weather conditions associated with low wind speeds, i.e. rather stagnant air, and fast photochemistry reducing the importance of horizontal transport in the boundary layer. Significant transport over larger distances (e.g. from highly polluted regions in adjacent countries to Switzerland as described in Schaub et al. (2005) for a frontal passage) is therefore considered to be unimportant for theses conditions.

SCIAMACHY NO_2 VTCs are converted to NO_x VTCs by employing representative values for the seasonal mean NO_2/NO ratio. The latter depends on the abundance of ozone and reactive organic compounds as well as on solar radiation and temperature. Thus, the ratio varies both spatially (horizontally and vertically) and seasonally. For the United States and based on 106 NO_x monitoring data sets measured at different distances from the predominant emission sources, Chu and Meyer (1991) recommended a national default value for the NO_2/NO ratio of 3. NO_x measurements operated since 1999 at an elevated rural site at the edge of the Swiss Plateau (Rigi, 47°04′ N, 8°28′ E, 1030 m a.s.l.) using a standard chemiluminescence detector for the measurement of NO and a photolytic converter for the selective conversion of NO_2 to NO (Steinbacher et al., 2007) indicate a seasonal variation of monthly mean ratios of between 1.6 (January) and 4.0 (August) for anticyclonic clear sky conditions and a time window between 10:00 and 12:00 UTC (Steinbacher, personal communication). Instead of using ratios from in-situ observations valid only for the altitude of the measurement site, we here apply seasonal mean tropospheric (0–8 km) column NO_2/NO ratios obtained from the TM4 model. The ratios are based on model output over Switzerland on clear days. Unfortunately, only output for 12:00 UTC (13:00 LT) was available. Nevertheless, these TM4 column ratios are assumed to be representative for the SCIAMACHY overpass time (10:00 LT) and are found to be surprisingly close to the ratios observed in situ at Mount Rigi. Vertical model profiles indicate that the NO_2/NO ratio changes only little in the lowest 1 to 2 km where most of the NO_2 resides, which likely explains the good agreement with the ratios measured at a single altitude. Above the planetary boundary layer, the ratios decrease rapidly but the free troposphere contributes only little to the total column above Switzerland.

The ratios finally applied are 3.0 (±0.7) for spring (MAM), 4.0 (±0.6) for summer (JJA), 2.8 (±1.0) for autumn (SON), and 1.5 (±0.5) for winter (DJF), where values in brackets represent the 1σ variability of the column ratios between individual days. The uncertainty in these ratios is added to the uncertainty in the SCIAMACHY NO_2 VTC to obtain an estimate for the uncertainty of the NO_x VTCs M finally used in the calculation of seasonal mean lifetimes according to Eq. (3). It is interesting to note that these ratios do not change significantly when cloudy days are included in the analysis, probably due to the compensating effects of reduced photolysis rates (increasing the ratio) and at the same time reduced O_3 concentrations (reducing the ratio) on cloudy days. Obtaining an emission rate E representative for the time of the SCIAMACHY overpass (10:00 LT corresponding to 09:00 UTC over Switzerland) is not straightforward due to the strong diurnal cycle in NO_x emissions. If NO_x has a short lifetime then only the emissions released during a few hours preceding the satellite overpass contribute to the NO_2 VTC measured by SCIAMACHY. If the lifetime is longer, however, then also emissions of the previous night and the previous day become relevant. This problem is illustrated in Fig. 2a showing the average diurnal cycle of NO_x emissions over Switzerland in winter (solid line). Also shown are the effective contributions of the emissions to the measured column if we assume three different NO_x lifetimes τ of 4, 10, and 20 h (dotted and dashed-dotted lines).

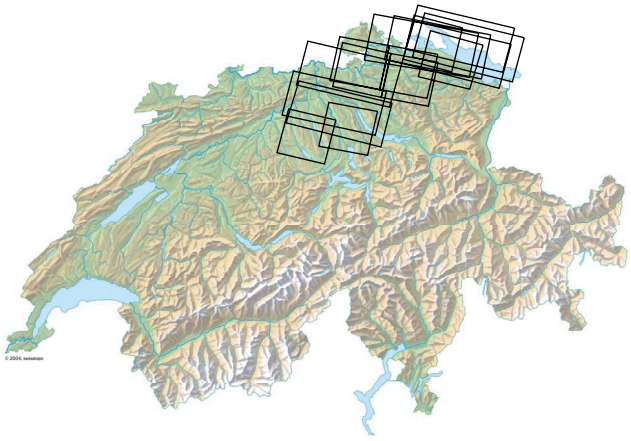

Fig. 3. Topographic map of Switzerland (© 2005 swisstopo) with the location of the SCIAMACHY pixels used for the pixel surface pressure sensitivity calculation.

The problem can be formulated as follows: The amount of NO_x released at a given hour t_i of the day over a period Δt=1 h (i.e. $E_i \cdot \Delta t$, where E_i is the emission rate at hour i given by the solid line in Fig. 2a) decays exponentially with a time constant τ. The column amount M accumulated by all emissions released during n-hours preceding the overpass can thus be expressed as:

$$M = \sum_{i=1}^{n} E_i \cdot e^{\frac{-(t_{SCIA}-t_i)}{\tau}} \cdot \Delta t, \quad (4)$$

where $t_{SCIA}-t_i$ is the time difference between the SCIAMACHY overpass and the NO_x release in hours. Values of $E_i \exp(-(t_{SCIA}-t_i)/\tau)$ are shown in Fig. 2a for three different lifetimes τ. Combining this equation with Eq. (3) we can compute an effective emission rate E_{eff} relevant for a given

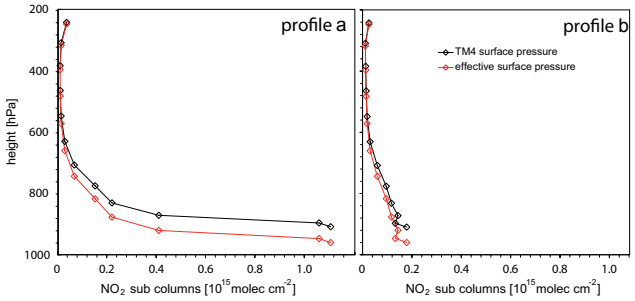

Fig. 4. CTM a priori NO_x profiles **(a)** (poor vertical mixing/polluted) and **(b)** (strong vertical mixing/remote) given as layer-specific sub columns. The black profiles are associated with the ECMWF/TM4 surface pressure at the location of the SCIAMACHY pixel. The red profiles are reaching down to the effective surface pressure calculated from the aLMo model with a $7\times7\,km^2$ resolution. For the examples shown here, surface pressures are taken from 10 March 2004 (profile a) and from 21 July 2001 (profile b).

lifetime τ as

$$E_{\text{eff}}(\tau)=\frac{\sum_{i=1}^{n} E_i \cdot e^{\frac{-(t_{\text{SCIA}}-t_i)}{\tau}} \cdot \Delta t}{\tau}. \quad (5)$$

Defining the weights $w_i=\exp(-(t_{\text{SCIA}}-t_i)/\tau)$ and noting that the sum $\sum_i w_i \cdot \Delta t=\tau$ we can rewrite Eq. (5) as

$$E_{\text{eff}}(\tau)=\frac{\sum_{i=1}^{n} E_i \cdot w_i}{\sum_{i=1}^{n} w_i}. \quad (6)$$

The effective emission rate is thus a weighted mean of the original emissions with weights given by an exponential decay with time constant τ. Values of E_{eff} are shown in Fig. 2b as a function of lifetime τ. For comparison, the daily mean emission rate is also shown (dashed line). For short lifetimes lower than about 7 h the effective emission rate is higher than the daily mean because only the high morning emissions including the early morning traffic peak are relevant. For longer lifetimes the low emission rates of the previous night become important reducing E_{eff} below the daily mean value. It is important to notice that the effective emission rate depends not only on the NO_x lifetime but also on the time of the satellite overpass. Such complicating effects need to be carefully considered for instance in NO_x emission inversion studies using a combination of model information and satellite observations to obtain improved emission estimates.

Now we are facing the problem that, for the calculation of lifetime τ according to Eq. (3), we have to use an effective emission rate which itself is depending on τ. This problem can be solved iteratively with

$$\tau_i=M/E_{\text{eff}}(\tau_{i-1}), \quad (7)$$

where in each step (i) the emission E_{eff} is adjusted to the lifetime obtained from the previous step $(i-1)$ using Eq. (6). The iteration is found to converge quickly within no more than 4 steps. Lifetime estimates based on this approach will be presented in Sect. 4.1.2.

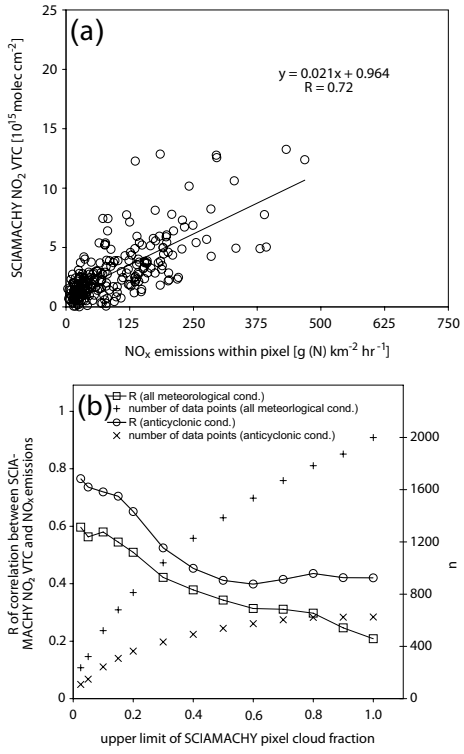

Fig. 5. Comparison between SCIAMACHY NO_2 VTCs (from 2003–2005) and collocated 09:00–10:00 UTC NO_x emission rates for pixels located entirely within the Swiss boundaries and anticyclonic clear sky meteorological conditions (pixel cloud fraction ≤ 0.1 n=243) **(a)**. Correlation coefficients of the present comparison as a function of different cloud fraction thresholds **(b)**.

3.2 Sensitivity of SCIAMACHY NO_2 VTCs to varying pixel surface pressure

As mentioned in Sect. 2.1 the mean pixel surface pressure is one of the parameters used in the column retrieval. In the TEMIS product this parameter is taken from the TM4 model to be consistent with the a priori NO_2 profile. It is therefore only available on a coarse resolution of $2°\times3°$ ($\sim220\times240\,km^2$) not resolving the complex topography of the Alpine region. The potential effects of this smoothed topography on NO_2 column retrievals over Switzerland will be demonstrated in Sect. 4.3 in terms of a sensitivity analysis. The following methods will be applied: For GOME and SCIAMACHY pixels with centre coordinates within the region of interest ROI_{CH} (Fig. 1) the deviations from the true topography are quantified. For this purpose the ECMWF/TM4 surface pressures p_{surf} are converted to altitude h_{surf} using daily profiles of pressure derived from ground based measurements at different altitudes in Switzerland. These values are then compared to the pixel averaged effective altitude h_{eff} based on the high resolution topography of the aLMo model (Alpine Model, the MeteoSwiss numerical weather prediction model) available on a resolution of $7\times7\,km^2$.

Table 1. Seasonal NO_x lifetime estimates based on a weighted orthogonal regression and lifetime-dependent effective emission rates for two different cloud fraction limits. Stated uncertainties correspond to the standard deviations of the slopes determined by the regression.

Cloud fraction limit	τ_{NO_x} (h) MAM (±std. dev.)	τ_{NO_x} (h) JJA (±std. dev.)	τ_{NO_x} (h) SON (± std. dev.)	τ_{NO_x} (h) DJF (± std. dev.)
0.1	4.93 (±1.39)	3.60 (±0.78)	6.10(±0.81)	13.12 (±3.78)
0.2	5.95 (±1.05)	3.64 (±0.60)	6.45 (±0.75)	16.04 (±3.16)

The sensitivity study is then carried out for a subset of clear sky SCIAMACHY pixels and two fixed a priori NO_2 profiles only. The AMF_{trop} and NO_2 VTCs are first calculated for the ECMWF/TM4 surface pressure p_{surf} as in the original retrieval and then recalculated for the effective surface pressure p_{eff} deduced from the aLMo topography h_{eff} using again the ground based vertical pressure profiles. The criteria for the pixel subset are i) anticyclonic clear sky meteorological conditions (Alpine Weather Statistics; MeteoSwiss, 1985), ii) pixel cloud fraction $\leq$0.1, and iii) a small standard deviation $<$65 m of the aLMo $7\times7\,km^2$ grid cell heights enclosed within a SCIAMACHY pixel, the latter ensuring that the reprocessing is done for pixels over a flat region in the vicinity of the Alps rather than directly over the mountains. The resulting SCIAMACHY pixels are located above the rather flat north-eastern Swiss Plateau (Fig. 3) but their surface pressure p_{surf} is still strongly influenced by the proximity of the Alps at the coarse ECMWF/TM4 resolution.

The sensitivity analysis is performed for two characteristic (and fixed) CTM a priori NO_2 profile shapes (Fig. 4). In a first profile (a), the bulk of NO_2 is residing near the ground. This profile is applied to pixels sampled during the cold part of the year (November-March) as it is expected to occur over polluted regions during the winter months when vertical mixing is generally weak or non-existing. The second profile (b) is applied to the subset of SCIAMACHY pixels sampled between April and August. It shows a much lower NO_2 abundance near the ground representing either a profile over a remote location or a summertime profile resulting from enhanced vertical mixing. As shown in Fig. 4 the use of a different surface pressure scales the profile vertically. The other retrieval (or forward model) parameters including surface albedo, cloud fraction and height, solar zenith angle and so on are kept constant.

4 Results and discussion

4.1 SCIAMACHY NO_2 VTCs versus NO_x emissions in Switzerland

4.1.1 Qualitative comparison

Figure 5a shows the comparison between SCIAMACHY NO_2 VTCs and the corresponding 09:00–10:00 UTC NO_x emission rates for anticyclonic clear sky (cloud fraction $\leq$0.1) conditions together with a simple linear regression (n=243). This simple comparison is limited by a number of factors: The relation between NO_2 VTCs and the corresponding NO_x emissions is expected to change with different meteorological conditions which influence the lifetime of NO_x as well as the NO_x/NO_2 column ratio. Even though the comparison is restricted to anticyclonic conditions, some transport of NO_x into and out of the column may still make a non-negligible contribution to the column budget. In addition, using emission rates from a fixed release time interval is not the best possible choice as discussed in Sect. 3.1.

Nevertheless, the resulting correlation coefficient of R=0.72 indicates that the collocated emissions explain more than 50% of the variance in the NO_2 VTCs. From this we may conclude that SCIAMACHY is able to observe the sources of air pollution from space even though its sensitivity is strongly decreasing towards the earth's surface.

Figure 5b shows the sensitivity of the correlation coefficient to the upper limit selected for the cloud fraction; i.e., only SCIAMACHY pixels with cloud fractions lower than or equal to this limit are taken into account. The comparison is carried out for all meteorological conditions (square symbols) as well as for anticyclonic conditions only (circles). The better correlations for the anticyclonic cases support our hypothesis that transport effects play a much smaller role under these conditions which are typically characterized by low wind speeds and rather homogeneous air masses (e.g. no passages of fronts). The general trend of decreasing correlations with increasing cloud fraction thresholds can be understood from clouds screening NO_2 located below. Moreover, in cloudy situations, the retrieved column is more strongly affected by the a priori assumption for the vertical NO_2 profile as was shown by Schaub et al. (2006). Note that the levelling off of the correlation coefficients for high upper cloud fraction limits in Fig. 5b is mainly due to the small number of cases that are additionally taken into account (denoted by the number of data points additionally shown in Fig. 5).

4.1.2 NO_x lifetime under anticyclonic clear sky conditions

As described in Sect. 3.1 the NO_x lifetime can be deduced from the slope of a correlation plot of NO_x columns M versus the corresponding emission rates E if both are provided in

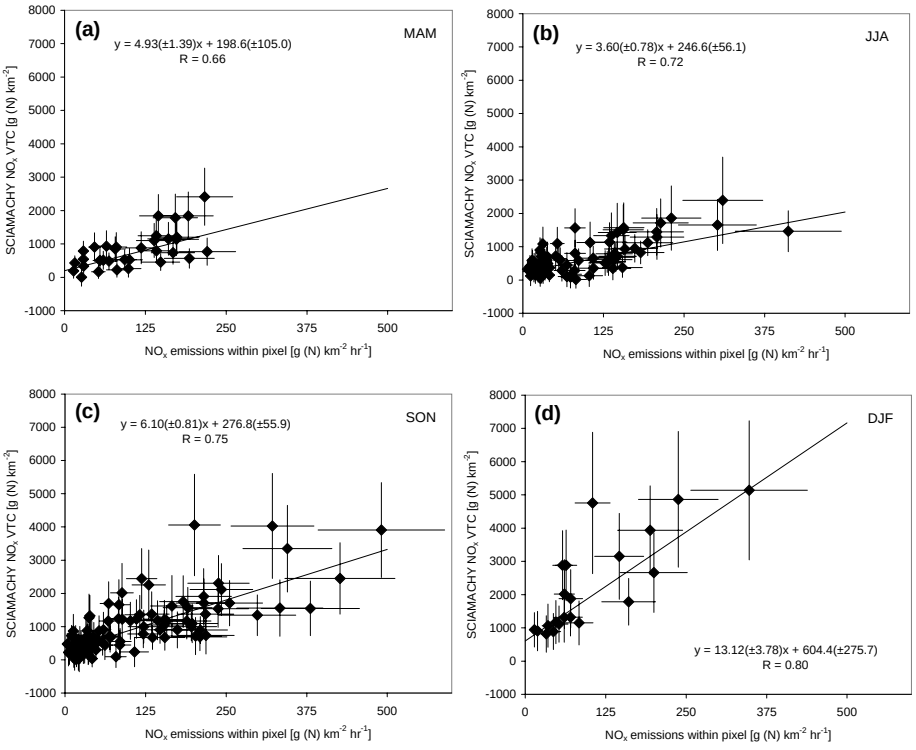

Fig. 6. Clear sky (cloud fraction≤0.1) SCIAMACHY NO_X VTCs located entirely within the Swiss boundaries versus iteratively calculated effective NO_X emission rates E_{eff}, see Eq. (7) for the four seasons spring **(a)**, summer **(b)**, fall **(c)** and winter **(d)**. NO_X VTCs are calculated from observed NO_2 VTCs using seasonal mean NO_2/NO column ratios. Additionally, the orthogonal regression output accounting for errors in both regression parameters is given. The slopes are the seasonal mean NO_X lifetimes in hours (see also Table 1).

suitable units. Instead of using emission rates from a fixed time interval as in the previous section, effective emission rates E_{eff} are used in the following calculated according to the iterative method described in Sect. 3.1.

The seasonal mean lifetimes are summarised in Table 1 and shown in Fig. 7 together with other estimates based on published data.

For summer, a large number of estimates is available

- from measurements in power plant plumes: 5 h (Ryerson et al., 1998), 2.8 and 4.2 h (Nunnermacker et al., 2000) and 6.4 h (Sillman, 2000),
- from measurements in urban plumes: Boston: 5.5 h (Spicer, 1982), Nashville: 2.0 h (Nunnermacker et al., 2000), Zurich: 3.2 h (Dommen et al., 1999),
- from GOME NO_2 VTCs above Germany: 6.0 h (Beirle et al., 2003) and
- zonal mean in the boundary layer (0–2 km) from the GEOS-CHEM CTM: 3.0 h (Martin et al., 2003).

For spring, Martin et al. (2003) calculated a mid-latitude NO_x lifetime from the GEOS-CHEM model of 8 h. For the winter season, Martin et al. (2003) and Beirle et al. (2003) reported on NO_x lifetimes of 19 and 21 h, respectively.

Additional NO_X lifetimes have been estimated here for the main daytime loss mechanism which is the oxidation of NO_2 by OH to form HNO_3. These estimates are based on pressure (∼960 hPa) and temperature values representative for the Swiss Plateau and on OH concentrations taken from the BERLIOZ and the SLOPE96 campaigns as well as from long-term OH measurements carried out at Hohenpeissenberg. The BERLIOZ campaign took place at a distance of 50 km from Berlin; the SLOPE96 campaign focused on polluted air masses travelling from the city of Freiburg to the Schauinsland Mountain (south-western Germany); the Hohenpeissenberg station is located in Southern Germany at an altitude of 985 m a.s.l. From a pollution point of view, all regions are similar to the conditions encountered over the Swiss Plateau. For an assumed temperature of 298 K and based on OH concentrations taken from the BERLIOZ and the SLOPE96 campaigns with noontime values of $(4–8)\times10^6$ cm^{-3} (Volz-Thomas et al., 2003; Mihelcic et al., 2003) and $(7–10)\times10^6$ cm^{-3} (Volz-Thomas and Kolahgar, 2000), respectively, the resulting mean daytime NO_X lifetimes in summer are estimated to be 4.6 h and 3.0 h. Seasonally averaged 09:00–10:00 UTC OH concentrations determined from clear sky OH measurements at Hohenpeissenberg carried out between 1999 and 2005 (Rohrer

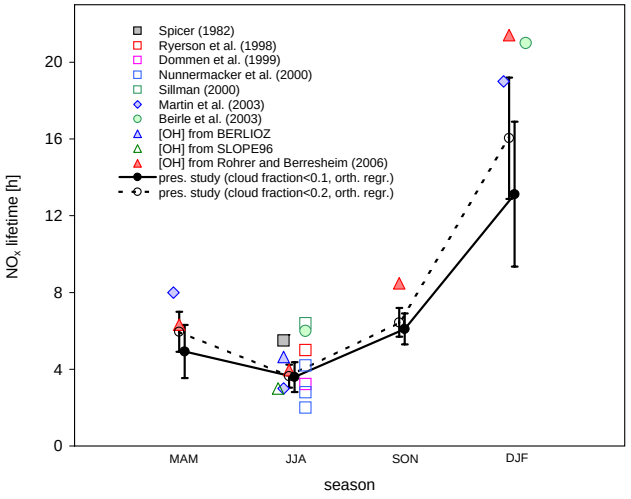

Fig. 7. Seasonal NO_x lifetimes (and standard deviations) over the Swiss Plateau under anticyclonic clear sky conditions estimated in this study. Results from other studies are shown for comparison. These data have been deduced from campaigns in the U.S. (Spicer, 1982; Ryerson et al., 1998; Nunnermacker et al., 2000; Sillman, 2000) and in the Swiss Plateau (Dommen et al., 1999), from GOME NO_2 VTCs over Germany (Beirle et al., 2003) and from the GEOS-CHEM model (Martin et al., 2003). Additionally, mean NO_x lifetimes against oxidation to HNO_3 are calculated for (i) 960 hPa and 298 K with OH concentrations of $(4–8)\times10^6$ cm^{-3} measured during the BERLIOZ campaign (Volz-Thomas et al., 2003; Mihelcic et al., 2003) and of $(7–10)\times10^6$ cm^{-3} measured during the SLOPE96 campaign (Volz-Thomas and Kolahgar, 2000) as well as for (ii) seasonally averaged OH concentrations measured by Rohrer and Berresheim (2006) with 960 hPa and assumed temperatures for the summer, spring/fall and winter seasons of 298 K, 288 K and 278 K, respectively.

and Berresheim, 2006; Berresheim, unpublished data, 2006) are used together with assumed temperatures for summer, spring/fall and winter of 298 K, 288 K and 278 K, respectively, to estimate NO_x lifetimes of 6.1, 3.9, 8.2 and 21.0 h for MAM, JJA, SON and DJF, respectively (Fig. 7).

Figure 6 shows for each season the SCIAMACHY NO_x columns for anticyclonic clear sky conditions plotted against the corresponding effective NO_x emission rates E_{eff}. Additionally, the linear fits obtained by the weighted orthogonal regression are shown. The relatively small intercepts suggest that under anticyclonic conditions the background NO_x plays a rather marginal role and the SCIAMACHY observations are dominated by the local NO_x emissions. The slopes of the linear fits correspond to the seasonal mean lifetimes. The effective emission rates used in the figure optimally correspond to these lifetimes as assured by the iterative adjustment (Eq. 7).

The comparison of our NO_x lifetimes with independent estimates generally shows a reasonable agreement though our values tend to be at the lower end, in particular in winter. A possible reason is that our estimates are only valid for clear sky situations. In Fig. 7 the dashed line shows additional lifetimes calculated for a higher cloud fraction limit of 0.2. For this higher threshold all lifetimes become larger (see also Table 1). The uncertainty ranges, on the other hand, become smaller because a larger number of data points can be included in the calculation of the slopes. A higher cloud fraction reduces the amount of solar radiation reaching the boundary layer. This in turn decreases the OH concentrations (Rohrer and Berresheim, 2006) which likely explains the larger lifetimes for the higher threshold. The Hohenpeissenberg OH data have been obtained for clear sky days with cloud fractions $\leq$1 octa (0.125), too. However, the wintertime lifetime estimate is significantly higher than the SCIAMACHY based estimate for a comparable cloud fraction of 0.1. This may be an indication that nighttime conversion to HNO_3 and deposition may be more important losses of NO_x in winter than reaction with OH during daytime. The lifetime estimates of Martin et al. (2003) represent monthly mean values not restricted to clear sky days. There is no obvious discrepancy from our estimates assuming that our values would become larger if even higher cloud fractions would be allowed.

All other estimates are implicitly representing clear sky or at least fair weather conditions, too. The different summertime estimates, for instance, were obtained in the framework of studies dedicated to the investigation of photochemical ozone production focussing on sunny days, or were derived from clear sky satellite observations. Our summertime value of about 3.6 h is well in the range of these estimates. In particular, it is in excellent agreement with another study carried out over Switzerland by Dommen et al. (1999) which obtained a lifetime of 3.2 h (Fig. 7).

Neglecting horizontal transport (smearing effect) could also contribute to an underestimation of lifetimes using our approach. Even though we are focussing on anticyclonic conditions, transport effects may still play a role in particular during winter when a long lifetime (>10 h) allows for transport over distances larger than the extension of SCIAMACHY pixels despite low wind speeds (<15 km/h).

4.2 Comparison of GOME and SCIAMACHY NO_2 VTCs over Switzerland

SCIAMACHY can better resolve regional structures of air pollution over Switzerland than GOME owing to the much smaller pixel size. This is demonstrated by Fig. 8 showing multi-annual mean NO_2 VTC distributions from (a) GOME (1996–2003) and (b) SCIAMACHY (2003–2005) mapped onto a fine $0.125°\times0.125°$ grid. For each grid cell a mean VTC has been computed by averaging over all clear sky pixels covering the given cell. Whereas the SCIAMACHY data can resolve the large contrast between the Alpine region (blue shadings) and the Swiss Plateau these differences are smeared out in the GOME data. In addition, SCIAMACHY

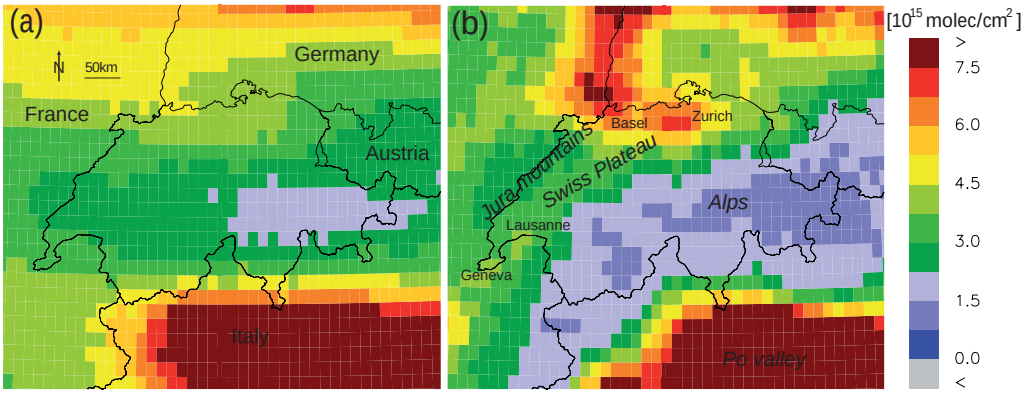

Fig. 8. Mean clear sky (satellite pixel cloud fraction $\leq$0.1) NO_2 tropospheric columns over the Central Alps and Switzerland deduced from GOME (1996–2003) **(a)** and SCIAMACHY (2003–2005) retrievals **(b)**. In contrast to the GOME picture, specific features such as the Alpine chain, the Jura Mountains, the Swiss Plateau and the areas of Greater Zurich and Basel clearly show up in the SCIAMACHY data.

can "see" individual population centres such as the areas of Zurich, Basel or the Rhine valley along the border between France and Germany. Elevated values are also seen around the cities of Lausanne and Geneva. All these details are missing in the GOME data. Interestingly, the area of Berne does not stand out even in the SCIAMACHY data, possibly due to the specific location of this city in between the Jura Mountains and the Alps.

For a more quantitative comparison seasonally averaged GOME and SCIAMACHY NO_2 VTCs have been calculated from all clear sky pixels with centre coordinates located within the region ROI_{SP} (see Fig. 1) covering the polluted regions of the Swiss Plateau (7° E – 9.5° E, 47° N – 47.75° N) only. Restricting the comparison to this region reduces the influence of the complex Alpine terrain as much as possible, which is particularly relevant for the large GOME pixels (Schaub et al., 2006). In Fig. 9a the resulting SCIAMACHY NO_2 VTCs are on average higher than the GOME columns in spring, summer and autumn. Somewhat higher values can be expected for SCIAMACHY because the extended GOME pixels always include less polluted regions outside of the Swiss Plateau. Surprisingly, the SCIAMACHY wintertime values are lower than the ones from GOME, the difference being more pronounced for the median than for the mean values. However, the GOME value in winter is only based on 7 individual pixels. Anticyclonic conditions are typically associated with the formation of fog over the Swiss Plateau during winter which likely explains the poor availability of clear sky pixels.

In order to improve the statistics the cloud fraction threshold has been relaxed to 0.2 in Fig. 9b. For this threshold a reasonable sample size of 32 pixels is available in winter. The differences between SCIAMACHY and GOME become significantly smaller in this case, not only in winter. The relative amplitude of the seasonal cycle (winter maximum – summer minimum), however, remains about 25% lower in the SCIAMACHY data as compared to GOME as highlighted in panel (c) where the values are scaled to the annual average. Again, the differences are more pronounced for the median values which are thought to be a more robust quantity as they are less susceptible to outliers.

For comparison, seasonally averaged NO_2 columns estimated from NO_2 data measured in situ between January 1997 and June 2003 at 15 ground-based sites at different altitudes in Switzerland and Southern Germany are also shown in Fig. 9c. The elevated sites are assumed to detect NO_2 concentrations representative for the appropriate height in the (free) troposphere over flat terrain. These measurements, together with boundary layer in situ measurements and an assumed mixing ratio of 0.02 ppb at 8 km, are used to construct NO_2 profiles. The latter are subsequently integrated to tropospheric NO_2 columns. Details on the data set and method are given in Schaub et al. (2006). For the present study, the ground-based in situ data set has been restricted to all clear sky days as flagged by the sunshine and high fog parameters from the Alpine Weather Statistics (MeteoSwiss, 1985). The columns are reaching down to an assumed mean Swiss Plateau height of 450 m a.s.l. The normalised seasonal variation of the ground-based data agrees reasonably well with the variation observed by GOME, in particular regarding the large differences between summer and winter. Similarly pronounced seasonal variations of space-borne NO_2 VTCs over industrialised regions have also been reported by Petritoli et al. (2004), Richter et al. (2005), van der A et al. (2006) and Uno et al. (2006). The seasonal amplitude in the SCIAMACHY data, however, is lower than in both GOME and ground-based observations: For the median values the amplitude is reduced by more than a factor of two. For the means the reduction is about 25% as mentioned earlier. This suggests that SCIAMACHY values over the Swiss Plateau are possibly underestimated in winter and/or overestimated in summer. It is important to note that this conclusion is only drawn here for the specific KNMI/BIRA retrieval. As has been shown by van Noije et al. (2006) there

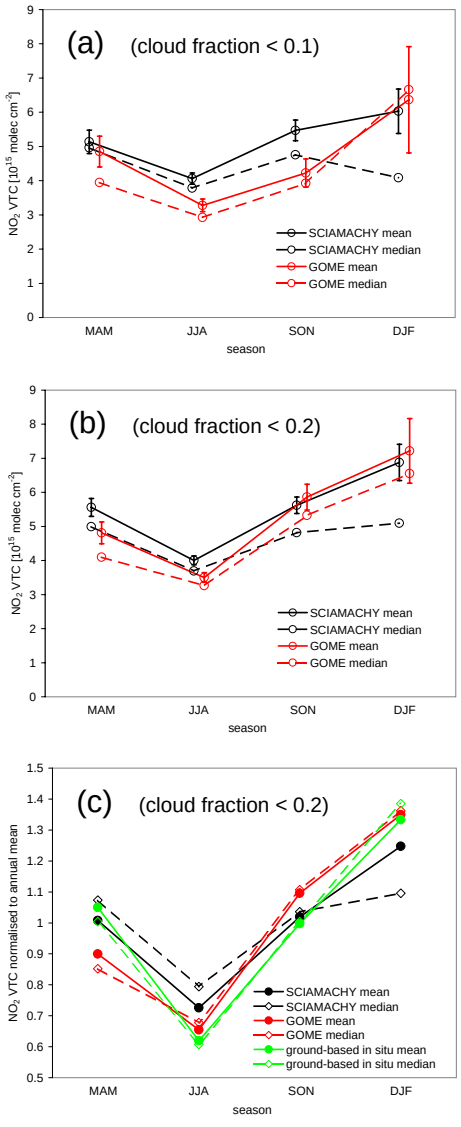

Fig. 9. Seasonal mean and median NO_2 VTCs from GOME and SCIAMACHY over the ROI_{SP} (Fig. 1) for cloud fractions $\leq$0.1. 76, 175, 129 and 86 SCIAMACHY pixels and 52, 95, 33 and 7 GOME pixels were available for the four seasons MAM, JJA, SON and DJF, respectively **(a)**. Same as above but for cloud fractions $\leq$0.2. Number of SCIAMACHY pixels per season: 144, 256, 236, and 141; GOME: 106, 154, 88, 32 **(b)**. Seasonal mean and median NO_2 VTCs from GOME, SCIAMACHY, and derived from ground-based in situ NO_2 measurements normalised to the annual mean value. Ground-based in situ columns were calculated following the method and data set described in Schaub et al. (2006) and for a Swiss Plateau ground elevation of 450 m a.s.l.. Number of in situ columns per season: 139, 165, 69 and 78 **(c)**.

are substantial differences in seasonal variations obtained by different groups using different retrieval algorithms. Moreover, our analysis is limited by the fact that SCIAMACHY and GOME have been sampled differently in space and time

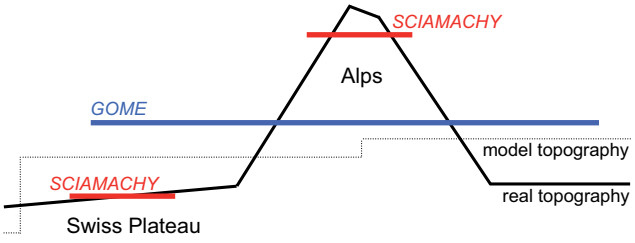

Fig. 10. Illustration of the problem arising for highly resolved satellite pixels over a marked topography when retrieved with coarsely resolved input parameters. The red and blue lines denote the averaged real surface height at the location of individual SCIAMACHY and GOME pixels, respectively. Further, the real topography and the topography given in a coarsely resolved global model are indicated. Over the large GOME pixel extension, the mean height given by a coarsely resolved model better approximates the averaged real surface height than for the smaller SCIAMACHY pixels.

and, thus, a perfect agreement is not expected. Nevertheless, the reduced seasonal cycle in SCIAMACHY data may be related to a problem in the retrieval over complex orography discussed in the next section.

4.3 Influence of inadequate treatment of Alpine surface topography on NO_2 VTC retrievals

4.3.1 GOME and SCIAMACHY pixel surface pressures

Errors of GOME NO_2 VTC retrievals were initially discussed by Richter and Burrows (2002) and Boersma et al. (2004). The methods and error budgets of the TEMIS retrievals applied to GOME, SCIAMACHY and OMI data are described in more detail in Blond et al. (2007) and Boersma et al. (2007). They reported on the following retrieval parameters inducing inaccuracies in the AMF calculation, which is the major error source for tropospheric retrievals over polluted regions: the a priori NO_2 profile shape, the surface albedo, cloud characteristics (fraction and height) and aerosol concentration. Here, we propose an additional source for systematic errors only relevant over complex topography: the mean surface pressure (or height) assumed for the retrieval of an individual pixel. This influence has not been investigated in the literature so far. As discussed in Sect. 3.2 the surface pressure p_{surf} used in the retrieval is obtained from the TM4 model at coarse resolution (ECMWF/TM4 surface pressure). While for large parts of the globe this will be sufficiently accurate, the low resolution may lead to problems over complex topography such as the Alpine region, in particular if there is a large mismatch in resolution between the satellite pixels and the surface pressure data set.

This is illustrated in Fig. 10 for the situation over the Alpine region. In a coarsely resolved model, the topography is averaged over extended grid elements, typically leading to an underestimation of the effective elevation of mountains

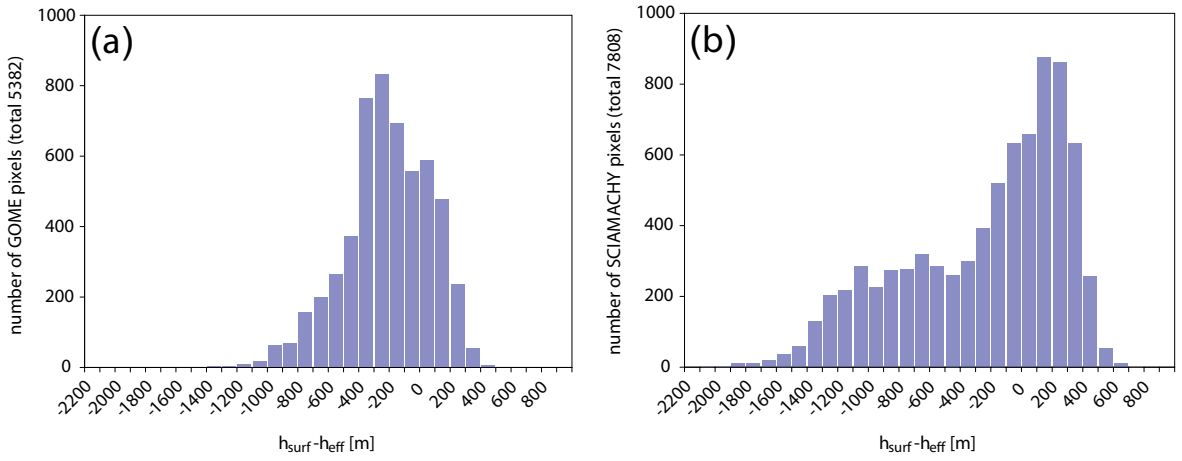

Fig. 11. Histogram distribution of the differences $h_{\text{surf}} - h_{\text{eff}}$ between pixel surface heights used in the retrieval and effective surface heights averaged over the pixels for all GOME (1996–2003) **(a)** and SCIAMACHY (2003–2005) **(b)** pixels with centre coordinates within ROI_{CH} (Fig. 1).

and an overestimation of the effective ground height in the surrounding area. Because the size of SCIAMACHY pixels is much smaller than the size of a model grid cell, it can be expected that the mean model heights h_{surf} (thin dotted line) show a larger deviation from the effective pixel-averaged surface heights h_{eff} for the smaller SCIAMACHY pixels (thick red lines) than for GOME (thick blue line).

Figure 11 presents histograms of the differences $\Delta\text{surf}=h_{\text{surf}} - h_{\text{eff}}$ between ECMWF/TM4 based surface elevations h_{surf} and effective heights h_{eff} for all GOME pixels of the years 1996–2003 and SCIAMACHY pixels of the years 2003–2005 (b) over the domain ROI_{CH} (Fig. 1). Figure 12 displays the corresponding pixel centre locations color-coded by the values of Δsurf. The following conclusions can be drawn:

– Due to the smoothed topography in ECMWF/TM4, the surface heights of the GOME and SCIAMACHY pixels are underestimated over the Alps and overestimated over the Swiss Plateau (Fig. 12).

– Lower minimum and higher maximum values of Δsurf are found for SCIAMACHY pixels (Figs. 11 and 12). This can be expected due to the smaller pixel size of SCIAMACHY compared to GOME (Fig. 10).

This demonstrates that certain retrieval parameters, such as the mean pixel surface pressure, can become increasingly inaccurate with increasing resolution of the satellite data if the spatial resolution of the parameters is not improved accordingly. In the following section, the effect of an inaccurate pixel surface pressure on the resulting NO_2 VTC is investigated for selected SCIAMACHY columns.

4.3.2 Sensitivity study for selected SCIAMACHY pixels

Figure 13 shows an idealized NO_2 profile over the Swiss Plateau where $h_{\text{surf}} > h_{\text{eff}}$. The profile which would be used in the retrieval reaching down to pressure p_{surf} is shown in black, the profile scaled to the higher effective surface pressure p_{eff} in red. Over the Alps the situation would be reversed. Following Eq. (1) (Sect. 2.1) and the formulation for the AMF_{trop} given there, the following systematic errors due to inaccurate surface heights are expected:

– For positive Δsurf ($h_{\text{surf}} > h_{\text{eff}}$; e.g. over the Swiss Plateau, Figs. 12) the near-ground NO_2 pollution is in reality located at a lower level than assumed in the retrieval. The retrieval therefore associates the high near-ground pollution with a too high sensitivity (thin dotted line in Fig. 13). This leads to an overestimated AMF_{trop} and, thus, to an underestimated NO_2 VTC.

– For negative Δsurf ($h_{\text{surf}} < h_{\text{eff}}$, e.g. over the Alps, Fig. 12) a tendency towards overestimation of the NO_2 VTCs is expected.

The effect of inaccurate pixel surface pressures is investigated for selected SCIAMACHY pixels following the method described in Sect. 3.2. Table 2 presents an overview of the selected pixels and the results obtained by the sensitivity analysis. For the selected pixels over the northeastern Swiss Plateau (see Fig. 3) the surface pressures p_{surf} and p_{eff} differ by about 50 hPa, corresponding to about 450 m.

The mean relative change in the AMF_{trop} due to the changing pixel surface pressure is $-27.2\pm1.3\%$ and $-11.7\pm1.8\%$ for the profile shapes A and B (Fig. 4), respectively. The mean relative change in the resulting NO_2 VTCs is $+37.5\pm2.4\%$ and $+13.3\pm2.4\%$, respectively. Obviously, the

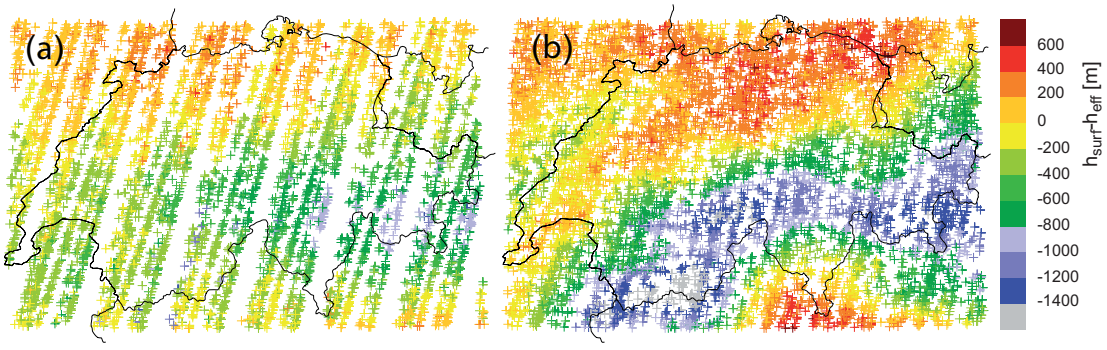

Fig. 12. Differences between pixel surface heights used in the retrieval and effective surface heights averaged over the respective pixels ($h_{surf} - h_{eff}$) for all GOME (1996–2003) **(a)** and SCIAMACHY (2003–2005) **(b)** pixels located over ROI_{CH} (Fig. 1). The ($h_{surf} - h_{eff}$) value for a pixel is indicated at its corresponding centre coordinate.

changes in the AMF_{trop} and the NO_2 VTCs due to changes in the pixel surface pressure are strongly dependent on the NO_2 profile shape.

These results are only a first attempt at quantifying these effects based on a limited subset of SCIAMACHY pixels and assumed a priori profile shapes. Depending on the NO_x emissions taking place at the pixel location, photochemical activity and prevailing meteorological conditions, real NO_2 profile shapes will differ from the ones used here. Nevertheless, given the distinctly different shapes A and B, the 13–38% NO_2 VTC error range appears to be a reasonable first estimate. For retrievals in the UV-visible spectral range with a significant decrease of the sensitivity towards the earth's surface, this effect is of major importance when the NO_2 resides close to the ground. As this situation most prominently occurs during the cold season this probably leads to an underestimation of NO_2 VTCs in winter and less so in other seasons. Hence, the reduced seasonal amplitude in SCIAMACHY data identified in Sect. 4.2 may be at least partly related to this problem.

At first glance, the problem seems to be less relevant for GOME as differences between true pressures and those used in the retrieval are smaller (Fig. 12a). Nevertheless, the complex topography over Switzerland probably leads to significant systematic errors, too. The reason is that NO_2 will not be evenly distributed within a GOME pixel covering parts of the Swiss Plateau and the Alps as in Fig. 10. Most of the measured NO_2 signal will originate from that part of the pixel located above the polluted Swiss Plateau for which there is still a discrepancy between true and ECMWF/TM4 altitude. If the contribution to the signal of the clean elevated part of the pixel would be zero then the relative error would be the same as for a SCIAMACHY pixel located entirely over the polluted part. However, since NO_2 VTCs over the Jura mountains and pre-Alps are well above zero there will probably be some compensation of the error since for these elevated regions the errors will be smaller or of opposite sign.

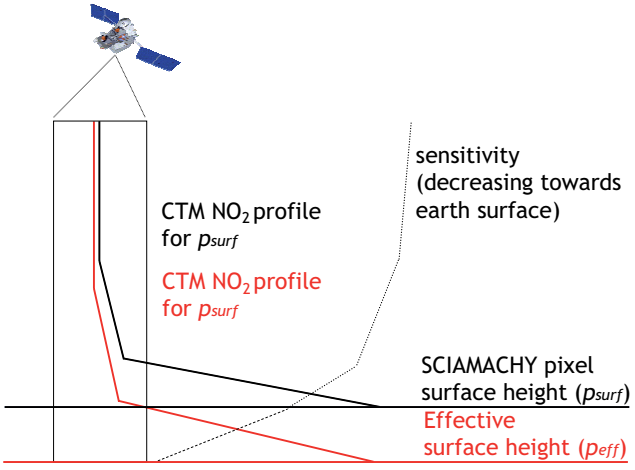

Fig. 13. Possible reason for too low SCIAMACHY NO_2 VTCs over the polluted Swiss Plateau: retrieval errors due to inaccurate pixel surface heights in regions with a marked topography.

5 Summary and conclusions

This study has evaluated SCIAMACHY NO_2 VTCs above Switzerland and the Alpine region. The clear relationship between a spatially and temporally highly resolved Swiss NO_x emission inventory and SCIAMACHY NO_2 columns under anticyclonic meteorological conditions has demonstrated the ability of SCIAMACHY to detect the main NO_x pollution features in Switzerland. The decreasing correlation between the two quantities when taking into account cloudy pixels indicates that SCIAMACHY is less likely to accurately detect sources of air pollution in cloudy situations. From the relation between the SCIAMACHY data and the NO_x emission inventory, seasonal NO_x lifetime estimates have been computed. This computation is complicated by the strong diurnal cycle in NO_x emissions which leads to a coupling between the estimated lifetimes and the relevant emission rate. A method has been demonstrated here solving this problem

Table 2. Results of sensitivity analysis of the effect of the inadequate representation of topography on selected SCIAMACHY pixels over the Swiss Plateau using two predefined a-priori NO_2 profiles for pixels sampled between November and March (Profile a) and between May and August (Profile b), respectively. For each pixel the tropospheric air mass factors AMF_{trop} obtained for the surface pressure p_{surf} used originally in the retrieval and for the pixel-averaged real pressure p_{eff} are shown. The last two columns are the resulting relative changes in both the AMF_{trop} and the NO_2 VTCs.

Date	Orbit, pixel number	Cloud fraction	p_{surf} from ECMWF/TM4 [hPa]	p_{eff} from aLMo (hPa)	AMF_{trop} calc. for p_{surf}	AMF_{trop} calc. for p_{eff}	rel. change AMF_{trop} (%)	rel. change NO_2 VTC (%)
Profile A (Fig. 4)								
10 Mar 04	71117	0.02	912.22	964.22	1.023	0.776	−24.1	+ 31.8
22 Jan 05	6574	0.01	903.92	956.62	1.315	0.941	−28.4	+ 39.7
22 Jan 05	6575	0.03	911.71	963.08	1.359	0.982	−27.7	+ 38.4
17 Nov 05	8731	0.01	899.13	948.72	1.326	0.958	−27.8	+ 38.4
17 Nov 05	8732	0.01	906.25	958.03	1.308	0.942	−28.0	+ 38.9
17 Nov 05	8764	0.01	895.73	950.36	1.315	0.944	−28.2	+ 39.3
23 Nov 05	7493	0.07	919.30	970.80	1.241	0.904	−27.2	+ 37.3
23 Nov 05	7559	0.00	912.22	958.68	1.257	0.916	−27.1	+ 37.2
26 Nov 05	7701	0.06	884.32	941.34	1.215	0.890	−26.7	+ 36.5
Profile B (Fig. 4)								
17 Apr 04	51383	0.01	899.71	953.97	1.109	0.972	−12.4	+ 14.1
12 May 04	7726	0.02	903.72	955.69	1.106	0.933	−15.6	+ 18.5
21 Jul 04	8674	0.01	913.20	963.67	1.004	0.889	−11.5	+ 12.9
21 Jul 04	8691	0.03	916.65	963.47	0.963	0.858	−10.9	+ 12.2
09 Aug 04	8645	0.01	905.58	959.25	0.936	0.835	−10.7	+ 12.1
03 Jul 05	8645	0.09	912.73	962.94	0.897	0.803	−10.5	+ 11.7
10 Aug 05	8614	0.01	905.79	962.17	0.895	0.801	−10.5	+ 11.7

using an iterative approach. A NO_x lifetime of 3.6±0.8 h has been obtained for summer, in good agreement with previous estimates and with lifetimes deduced from published OH concentrations measured during daytime. In winter, the lifetime is much longer on the order of 13.1±0.8 h to 16.0±3.2 h for cloud fraction limits of 0.1 and 0.2, respectively. The larger lifetime for the higher threshold is consistent with fewer OH radicals being present during more cloudy conditions. These values are lower than previous estimates but no firm conclusion can be drawn due to the small number of data available for comparison in winter. Nevertheless, an underestimation of the wintertime NO_x lifetime based on the SCIAMACHY measurements can not be ruled out.

A comparison of SCIAMACHY and GOME NO_2 VTCs has shown the advantage of better resolved space-borne data with regard to monitoring the NO_2 pollution distribution on a regional scale. However, the quantitative comparison of multi-year seasonal averages provides evidence for a reduced amplitude in the seasonal cycle of SCIAMACHY with comparatively high values in summer and low values in winter. This has further been supported by a comparison with the seasonal variation of NO_2 VTCs derived from ground-based in situ measurements which shows a better agreement with GOME.

A problem likely contributing to an underestimation of SCIAMACHY NO_2 VTCs over the Swiss Plateau in winter is the use of inaccurate satellite pixel surface pressures derived from a coarse resolution global model in the retrieval. It has been found that the marked topography in the Alpine region can lead to deviations of several hundred meters between assumed and pixel-averaged real surface heights. The sensitivity of the retrieved NO_2 VTCs to this problem has been estimated based on selected clear sky SCIAMACHY pixels over the Swiss Plateau and two predefined a priori NO_2 profile shapes. An effect of 10–15% has been found for the profile characteristic of summer conditions and of 30–40% for the winter profile. In winter, large concentrations of NO_x are accumulating near the surface due to reduced vertical mixing and a long lifetime. Together with the strongly decreasing sensitivity of UV/VIS instruments towards the surface this results in an enhanced sensitivity to surface pressure errors in winter. Our lifetime estimates for winter may thus be regarded as lower limits. The true lifetimes may be up to 40% higher as they proportionally scale with the NO_2 columns. Yet, a more accurate quantification will require a complete reprocessing of the SCIAMACHY data with improved surface pressure data. This was out of the scope of the present study.

Even though differences between surface pressures used in the retrieval and pixel-averaged real pressures are smaller for the larger GOME pixels, the GOME measurements over Switzerland likely suffer from systematic errors as well: For a GOME pixel located partly over the Swiss Plateau and partly over the Alps only the polluted Swiss Plateau will make a significant contribution to the measured NO_2 signal and for this part the pixel-averaged surface height is not

representative. It is thus unlikely that the inadequate description of the Alpine topography is the only reason for the different amplitudes of the seasonal cycle observed by GOME and SCIAMACHY.

For the purpose of air pollution monitoring on a regional scale, highly resolved space-borne data are of great value. However, we further conclude from this study that in order to fully exploit the potential of such data, the forward parameters used in the retrieval should be available on a scale matching the size of the satellite pixels. This not only applies to surface pressure but also to albedo and a-priori NO_2 profiles. This is of increasing importance with regard to the decreasing pixel sizes of new instruments from $320\times40\,km^2$ (GOME) to $60\times30\,km^2$ (SCIAMACHY) to $13\times24\,km^2$ (OMI).

Acknowledgements. This work was funded by the Swiss Federal Office for the Environment (FOEN) and supported through ACCENT/Troposat-2. For providing information on ground-based NO_2 measurements in Switzerland we acknowledge the Swiss National Air Pollution Monitoring Network (NABEL) and M. Steinbacher. TM4 model data used for the computation of NO_2/NO column ratios have been generated within the EU project QUANTIFY and were kindly provided by E. Meijer and P. van Velthoven (KNMI). Furthermore we thank I. DeSmedt and M. Van Roozendael (BIRA/IASB) and H. Eskes and R. van der A (KNMI) for their work on making available the TEMIS GOME and SCIAMACHY NO_2 data set used in this study, and the two referees who substantially contributed to the improvement of the manuscript.

Edited by: T. Wagner

References

Beirle, S., Platt, U., Wenig, M., and Wagner, T.: Weekly cycle of NO_2 by GOME measurements: a signature of anthropogenic sources, Atmos. Chem. Phys., 3, 2225–2232, 2003, http://www.atmos-chem-phys.net/3/2225/2003/.

Beirle, S., Platt, U., Wenig, M., and Wagner, T.: Highly resolved global distribution of tropospheric NO_2 using GOME narrow swath mode data, Atmos. Chem. Phys., 4, 1913–1924, 2004, http://www.atmos-chem-phys.net/4/1913/2004/.

Blond, N., Boersma, K. F., Eskes, H. J., van der A, R. J., Van Roozendael, M., De Smedt, I., Bergamatti, G., and Vautard, R.: Intercomparison of SCIAMACHY nitrogen dioxide observations, in situ measurements and air quality modeling results over Western Europe, J. Geophys. Res., 112, D10311, doi:10.1029/2006JD007277, 2007.

Boersma, K. F., Eskes, H. J., and Brinksma, E. J.: Error analysis for tropospheric NO_2 retrieval from space, J. Geophys. Res., 109, D04311, 2004.

Boersma, K. F., Eskes, H. J, Veefkind, J. P., Brinksma, E. J.,van der A, R. J., Sneep, M., van den Oord, G. H. J., Levelt, P. F., Stammes, P., Gleason, J. F., and Bucsela, E. J.: Near-real time retrieval of tropospheric NO2 from OMI, Atmos. Chem. Phys., 7, 2103–2118, 2007, http://www.atmos-chem-phys.net/7/2103/2007/.

Bovensmann, H., Burrows, J. P., Buchwitz, M., Frerick, J., Noël, S., and Rozanov, V. V.: SCIAMACHY: Mission objectives and measurement modes, J. Atmos. Sci., 56, 2, 127–150, 1999.

Burrows, J. P., Weber, M., Buchwitz, M., Rozanov, V., Ladstätter-Weissenmayer, A., Richter, A., DeBeek, R., Hoogen, R., Bramstedt, K., Eichmann, K. U., Eisinger, M., and Perner, D.: The global ozone monitoring experiment (GOME): Mission concept and first scientific results, J. Atmos. Sci., 56, 151–175, 1999.

Chu, S. H. and Meyer, E. L.: Use of ambient ratios to estimate impact of NO_x sources on annual NO_2 concentrations, Proceedings, 84. Annual Meeting and Exhibition of the Air and Waste Management Association, Vancouver, B.C., 16–21 June 1991,91–180.6, 16 pp., 1991.

Dentener, F. J. and Crutzen, P. J.: Reaction of N_2O_5 on tropospheric aerosols: impact on the global distributions of NO_x, O_3 and OH, J. Geophys. Res., 98, 7149–7163, 1993.

Dentener, F. J., van Weele, M., Krol, M., Houweling, S., and van Velthoven, P.: Trends and inter-annual variability of methane emissions derived from 1979–1993 global CTM simulations, Atmos. Chem. Phys., 3, 73–88, 2003, http://www.atmos-chem-phys.net/3/73/2003/.

Dommen, J., Prévôt, A. S. H., Hering, A. M., Staffelbach, T., Kok, G. L., and Schillawski, R. D.: Photochemical production and aging of an urban air mass, J. Geophys. Res., 104, D5, 5493–5509, 1999.

Eskes, H. J.: Combined retrieval, modeling and assimilation approach to GOME NO_2, in GOA final report, European Commission 5th framework programme 1998–2002, EESD-ENV-99-2, 116–122, Eur. Comm., De Bilt, Netherlands, 2003.

Finlayson-Pitts, B. J. and Pitts, J. N.: Chemistry of the upper and lower Atmosphere – Theory, Experiments and Applications, Academic Press, San Diego, CA, 2000.

FOEN (Swiss Federal Office for the Environment, BAFU): Vom Menschen verursachte Luftschadstoffemissionen in der Schweiz von 1900 bis 2010, Schriftenreihe Umwelt Nr. 256, 1995.

FOEN (Swiss Federal Office for the Environment, BAFU): NABEL – Luftbelastung 2004, Schriftenreihe Umwelt Nr. 388, 2005.

Hueglin, C., Buchmann, B., and Weber, R. O.: Long-term observation of real-world road traffic emission factors on a motorway in Switzerland, Atmos. Environ., 40, 3696–3709, 2006.

IPCC, Climate Change 2001: The Scientific Basis, Contribution of Working Group I to the Third Assessment Report of the Intergovernmental Panel on Climate Change, Cambridge University Press, Cambridge, UK and New York, USA, 2001.

Jaeglé, L., Jacob, D. J., Wang, Y., Weinheimer, A. J., Ridley, B. A., Campos, T. L., Sachse, G. W., and Hagen, D. E.: Sources and chemistry of NO_x in the upper troposphere over the United States, Geophys. Res. Lett., 25, 1705–1708, 1998.

Keller, J., Andreani-Aksoyoglu, S., Tinguely, M., and Prévôt, A. S. H.: Emission Scenarios 1985–2010: Their Influence on Ozone in Switzerland, PSI Bericht Nr. 05–07, Paul Scherrer Institut, Villigen PSI, 2005.

Keller, M. and Zbinden, R.: Luftschadstoffemissionen des Strassenverkehrs 1980–2030, Schriftenreihe Umwelt Nr. 355, FOEN (Swiss Federal Office for the Environment), 2004.

Koelemeijer, R. B. A., Stammes, P., Hovenier, J. W., and de Haan, J. F.: A fast method for retrieval of cloud parameters using oxygen A-band measurements from Global Ozone Monitoring Experiment, J. Geophys. Res., 106, 3475–3490, 2001.

Kramm, G., Dlugi, R., Dollard, G. J., Foken, T., Mölders, N., Müller, H., Seiler, W., and Sievering, H.: On the dry deposition of ozone and reactive nitrogen species, Atmos. Environ., 29, 3209–3231, 1995.

Kühlwein, J.: Uncertainties in the arithmetical determination of pollutant emissions from road traffic and demands on future models, PhD thesis, University of Stuttgart, 2004.

Kühlwein, J. and Friedrich, R.: Uncertainties of modelling emissions from road transport, Atmos. Environ., 34, 4603–4610, 2000.

Kunhikrishnan, T., Lawrence, M. G., von Kuhlmann, R., Richter, A., Ladstätter-Weissenmayer, A., and Burrows, J. P.: Analysis of tropospheric NO_x over Asia using the model of atmospheric transport and chemistry (MATCH-MPIC) and GOME-satellite observations, Atmos. Environ., 38, 581–596, 2004.

Leue, C., Wenig, M., Wagner, T., Klimm, O., Platt, U., and Jahne, B.: Quantitative analysis of NO_x emissions from Global Ozone Monitoring Experiment satellite image sequences, J. Geophys. Res., 106, 5493–5505, 2001.

Martin, R. V., Jacob, D. J., Chance, K., Kurosu, T. P., Palmer, P. I., and Evans, M. J.: Global inventory of nitrogen oxide emissions constrained by space-based observations of NO_2columns, J. Geophys. Res., 108, D17, 4537, doi:10.1029/2003JD003453, 2003.

MeteoSwiss: Alpine Weather Statistics (Alpenwetterstatistik – Witterungskalender: Beschreibung der einzelnen Parameter), MeteoSwiss, Switzerland, 1985.

Mihelcic, D., Holland, F., Hofzumahaus, A., Hoppe, L., Konrad, S., Müsgen, P., Pätz, H.-W., Schäfer, H.-J., Schmitz, T., Volz-Thomas, A., Bächmann, K., Schlomski, S., Platt, U., Geyer, A., Alicke, B., and Moortgat, G. K.: Peroxy radicals during BERLIOZ at Pabsttum: measurements, radical budgets and ozone production, J. Geophys. Res., 108, D4, 8254, doi:10.1029/2001JD001014, 2003.

Nunnermacker, L. J., Kleinman, L. I., Imre, D., Daum, P. H., Lee, Y.-N., Lee, J. H., Springston, S. R., and Newman, L.: NO_y lifetimes and O_3 production efficiencies in urban and power plant plumes: analysis of field data, J. Geophys. Res., 105, D7, 9165–9176, 2000.

Palmer, P. I., Jacob, D. J., Chance, K., Martin, R. V., Spurr, R. J. D., Kurosu, T. P., Bey, I., Yantosca, R., Fiore, A., and Li, Q.: Air mass factor formulation for spectroscopic measurements from satellites: Application to formaldehyde retrievals from the Global Ozone Monitoring Experiment, J. Geophys. Res., 106, 14 539–14 550, 2001.

Palmer, P. I., Jacob, D. J., Fiore, A. M., Martin, R. V., Chance, K., and Kurosu, T. P.: Mapping isoprene emissions over North America using formaldehyde column observations from space, J. Geophys. Res., 108, D6, 4180, doi:10.1029/2002JD002153, 2003.

Petritoli, A., Bonasoni, P, Giovanelli, G., Ravegnani, F., Kostadinov, I., Bortoli, D., Weiss, A., Schaub, D., Richter, A., and Fortezza, F.: First comparison between ground-based and satellite-borne measurements of tropospheric nitrogen dioxide in the Po basin, J. Geophys. Res., 109, D15307, doi:10.1029/2004JD004547, 2004.

Platt, U.: Differential optical absorption spectroscopy (DOAS), Chem. Anal. Series, 127, 27–83, 1994.

Richter, A. and Burrows, J. P.: Tropospheric NO_2 from GOME measurements, Adv. Space Res., 29, 1673–1683, 2002.

Richter, A., Burrows, J. P., Nüss, H., Granier, C., and Niemeier, U.: Increase in tropospheric nitrogen dioxide over China observed from space, Nature, 437, doi:10.1038/nature04092, 2005.

Rohrer, F. and Berresheim, H.: Strong correlation between levels of tropospheric hydroxyl radicals and solar ultraviolet radiation, Nature, 442, 184–187, 2006.

Ryerson, T. B., Buhr, M. P., Frost, G. J., Goldan, P. D., Holloway, J. S., Hübler, G., Jobson, B. T., Kuster, W. C., McKeen, S. A., Parrish, D. D., Roberts, J. M., Sueper, D. T., Trainer, M., Williams, J., and Fehsenfeld, F. C.: Emissions lifetimes and ozone formation in power plant plumes, J. Geophys. Res., 103, D17, 22 569–22 583, 1998.

Schaub, D., Boersma, K. F., Kaiser, J. W., Weiss, A. K., Eskes, H. J., and Buchmann, B.: Comparison of GOME tropospheric NO_2 columns with NO_2 profiles deduced from ground-based in situ measurements, Atmos. Chem. Phys., 6, 3211–3229, 2006, http://www.atmos-chem-phys.net/6/3211/2006/.

Schaub, D., Weiss, A. K., Kaiser, J. W., Petritoli, A., Richter, A., Buchmann, B., and Burrows, J. P.: A transboundary transport episode of nitrogen dioxide as observed from GOME and its impact in the Alpine region, Atmos. Chem. Phys., 5, 23–37, 2005, http://www.atmos-chem-phys.net/5/23/2005/.

Seinfeld, J. H. and Pandis, S. N.: Atmospheric chemistry and physics – from air pollution to climate change, John Wiley and Sons, New York, 1998.

Sillman, S.: Ozone production efficiency and loss of NO_x in power plant plumes: photochemical model and interpretation of measurements in Tennessee, J. Geophys. Res., 105, D7, 9189–9202, 2000.

Solomon, S., Portmann, W., Sanders, R. W., Daniel, J. S., Madsen, W., Bartram, B., and Dutton, E. G.: On the role of nitrogen dioxide in the absorption of solar radiation, J. Geophys. Res., 104, 12 047–12 058, 1999.

Spicer, C. W.: Nitrogen oxide reactions in the urban plume of Boston, Science, 215, 4536, 1095–1097, 1982.

Stammes, P.: Spectral radiance modelling in the UV-Visible Range, in IRS 2000: Current problems in Atmospheric Radiation, Edited by: Smith, W. L. and Timofeyev, Y. M.: A. Deepak Publ., Hampton (VA), 2001.

Steinbacher, M., Zellweger, C., Schwarzenbach, B., Bugmann, S., Buchmann, B., Ordoñez, C., Prevot, A. S. H., and Hueglin, C.: Nitrogen dioxide measurements at rural sites in Switzerland: Bias of conventional measurement techniques, J. Geophys. Res., 112, D11307, doi:10.1029/2006JD007971, 2007.

Uno, I., He, Y., Ohara, T., Yamaji, K., Kurokawa, J.-I., Katayama, M., Wang, Z., Noguchi, K., Hayashida, S., Richter, A., and Burrows, J. P.: Systematic analysis of interannual and seasonal variations of model-simulated tropospheric NO_2 in Asia and comparison with GOME-satellite data, Atmos. Chem. Phys. Disc., 6, 11 181–11 207, 2006.

van der A, R. J., Peters, D. H. M. U., Eskes, H., Boersma, K. F., Van Roozendael, M., De Smedt, I., and Kelder, H. M.: Detection of the trend and seasonal variation in tropospheric NO_2 over China, J. Geophys. Res., 111, D12317, doi:10.1029/2005JD006594, 2006.

Vandaele, A. C., Fayt, C., Hendrick, F., et al.: An intercomparison campaign of ground-based UV-visible measurements of NO_2, BrO, and OClO slant columns: Methods of anal-

ysis and results for NO_2, J. Geophys. Res., 110, D08305, doi:10.1029/2004JD005423, 2005.

van Noije, T. P. C., Eskes, H. J., Dentener, F. J. , Stevenson, D. S., et al.: Multi-model ensemble simulations of tropospheric NO_2 compared with GOME retrievals for the year 2000, Atmos. Chem. Phys., 6, 2943–2979, 2006, http://www.atmos-chem-phys.net/6/2943/2006/.

Volz-Thomas, A., Geiss, H., Hofzumahaus, A., and Becker, K.-H.: Introduction to special section: photochemistry experiment in BERLIOZ, J. Geophys. Res., 108, D4, 8252, doi:10.1029/2001JD002029, 2003.

Volz-Thomas, A. and Kolahgar, B: On the budget of hydroxyl radicals at Schauinsland during the Schauinsland Ozone Precursor Experiment (SLOPE96), J. Geophys. Res., 105, D1, 1611–1622, 2000.

York, D.: Least-square fitting of a straight line, Can. J. Phys., 44, 1079–1086, 1966.